Sixth International Symposium on Turbulence and Shear Flow Phenomena
Seoul, Korea, 22-24 June 2009

FLOW BEHAVIOR OF SUPERSONIC IMPINGING MOIST AIR JETS

ALAM Miah Md. Ashraful
Graduate School of Science and Engineering
Saga University
1 Honjo-machi, Saga-shi, Saga, 840-8502, JAPAN
08633101@edu.cc.saga-u.ac.jp

MATSUO Shigeru & SETOGUCHI Toshiaki
Department of Mechanical Engineering
Saga University
1 Honjo-machi, Saga-shi, Saga, 840-8502, JAPAN
matsuo@me.saga-u.ac.jp; setoguci@me.saga-u.ac.jp

KIM Heuy Dong
School of Mechanical Engineering
Andong National University
388, Songcheon-dong, Andong 760-749, KOREA
kimhd@adu.ac.kr

ABSTRACT

Pronounced aeroacoustic resonances are exhibited in the flowfield where a jet emerges from an orifice or a nozzle and impinges on a solid surface. One instance where such resonances are produced is in a high speed jet impingement, such as in the space launch vehicle systems, multi-stage rocket separation, jet-engine exhaust impingement, terrestrial rocket launch, and in the next generation short take off and vertical landing (STOVL) aircraft, etc. Supersonic impinging jets produce a highly unsteady flowfields leading to a drastic increase of noise level with very high dynamic pressure loads and thermal loads on nearby surfaces. These high-pressure, high-temperature and acoustic loads are also accompanied by dramatic lift loss, severe ground erosion and hot gas ingestion to the inlet in the jet engines aircraft. Previous studies of supersonic impinging jets suggest that the highly unsteady behavior of the impinging jets is due to a feedback loop between the fluid and acoustic fields, which leads to these adverse effects. In actual jet flow, the working gas may contain condensable gas such as steam or moist air. In these cases, the non-equilibrium condensation may occur at the region between nozzle exit and an object. The jet flow with non-equilibrium condensation may be quite different from that without condensation. Therefore, in this study, the effect of the non-equilibrium condensation of moist air on the axisymmetric under-expanded supersonic impinging jet on a vertical flat plate was investigated numerically.

INTRODUCTION

Supersonic jet impingements, on solid boundaries, generally result an extremely unsteady flowfields accompanied by a host of undesirable aeroacoustic properties. These include, but are not limited to, very high ambient noise levels dominated by discrete frequency tones -referred to as impingement tones- and the high speed and temperature leads to a severe mechanical and thermal loading on the impinging plate. These impingement tones may cause sonic fatigue of the structures and also may damage various instruments and equipments. Moreover, these high-pressure, high-temperature and acoustic loads are also accompanied by dramatic lift loss, severe ground erosion and hot gas ingestion.

Unfortunately, supersonic impinging jets are ubiquitously present in a wide variety of situations, such as in the space launch vehicle systems, the supersonic short take-off and landing (STOVL) aircraft (Petrie, 1980) where the exhaust jet is deflected downwards by a wing with trailing edge flaps, multi-stage rocket separation, deep-space docking, jet-engine exhaust impingement, gas-turbine failure, and terrestrial rocket launch, and so on. Moreover, in some manufacturing industries, free jets also require to impinge upon solid boundaries, such as in laser cutting, surface cooling, materials removal, paint spraying, etc. Despite the simple geometry, the flow structure of supersonic impinging jet onto a flat plate is rather complex; it contains mixed supersonic and subsonic regions, and involves interaction of shock and expansion waves with jet shear layers (Lamont and Hunt, 1980; Kim and Park, 2005). Impinging jets are characterized by a strong coupling between the flow and acoustic fields and a self-contained feedback mechanism that result in high amplitude of sound tones. The feedback loop begins with the formation of turbulence structures within the shear layer of the jet. These structures grow and convect downstream where they interact with the impingement plate. Acoustic waves are created due to this interaction and travel outside of the flow in the upstream direction. These acoustic waves/perturbations eventually reach the receptivity location of the shear layer at the nozzle exit where they excite the shear layer and lead to the formation of more structures, thus perpetuating the cycle. The initial formation of turbulence structures within the shear layer is largely dependent on the frequency(ies) of forcing. The development of structures is further influenced by the strong interaction between the flow and the plate.

In supersonic impinging jets, the high speed and temperature leads to a severe mechanical and thermal loading on the impinging plate. It becomes oscillatory under certain

operating conditions after the initial transient impinging behavior. The unsteady oscillation can make thermal and mechanical loading more severe. An oscillatory supersonic impinging jet produces severe noise at discrete frequencies, which may cause sonic fatigue of the structures and also may damage various instruments and equipments. The unsteady oscillatory nature is caused by the feedback loop of the downstream traveling vortical structures and the upstream propagating acoustic waves (Krothapalli, 1985; Powell, 1988; Tam and Ahuja, 1990). The energy of the feedback loop is provided by the instability waves in the shear layer of the jet. Upon interacting with the impinging surface, the downstream traveling coherent jet structures generate strong pressure fluctuations near the impingement region that lead to acoustic waves in the near sound field. The structure of impinging jet depends on the design Mach number, that is, nozzle geometry, nozzle pressure ratio, the distance between nozzle exit and flat plate and so on.

In the above mentioned applications, usually the working gas is steam or moist air, which have not yet received the same level of attention in supersonic jet technologies as single-phase gases. In these cases, the non-equilibrium condensation (Wegener and Mack, 1958; Matsuo et al., 1985) may occur at the region between nozzle exit and an object. In the supersonic flow with the condensation, the surrounding gas will be heated by the release of latent heat of condensation. The jet flow with non-equilibrium condensation may be quite different from that without condensation. However, the study for the effect of non-equilibrium condensation on the flow behavior such as wave structure of supersonic impinging jet, static pressure on a solid body and so on, are not investigated satisfactorily till now. It is required to perform more investigation to find out the effect of non-equilibrium condensation on the oscillatory behavior, wave structure of supersonic impinging jet and also the effect of varying nozzle pressure ratio.

The principal thrust of the present computational work is to acquire an in-depth understanding of the unsteady flow characteristics, the surface pressure oscillation and the structural changes of oscillatory flow of axisymmetric supersonic under-expanded jets issuing from a converging nozzle at moderate nozzle pressure ratios which impinges on a vertical flat plate are to be presented. Moreover, we are going to focus on the effect of non-equilibrium condensation of moist air on the jet flow behavior and acoustic waves by varying relative humidity of air and also with varying nozzle pressure ratios.

NUMERICAL APPROACHES

Numerical schemes

Assumptions used in this present numerical simulation of the two phase supersonic impinging jet flow are as follows ; Both velocity slip and temperature difference do not exist between condensate particles and gas mixture, and the effect of the condensate particles on pressure is neglected. The two-dimensional multi-phase viscous flow solver is used for these computations, is developed at our laboratory. It is based on the compressible Reynolds and Favre-averaged Navier-Stokes equations and droplet growth equation (Sislian, 1975) using modified Goldberg's $k-R$ turbulence models (Goldberg, 1994a; Goldberg, 1996b; Heiler, 1999) for closure. Finite-difference method is used for the spatial Discretization of the conservation equations. The inviscid fluxes are calculated with the upwind flux-difference splitting method of Roes Approximate Riemann solver. The MUSCL technique (Yee, 1989) is applied to achieve a spatial accuracy of second or third order. In regions with large gradients the order is limited by a TVD-limiter to avoid numerical instabilities. A second order-central difference scheme is applied to calculate the viscous fluxes and the Split MacCormack (1969) scheme, a second-order fractional step, is employed for time integration. In the present simulation, nucleation rate, critical droplet radius, surface tension, saturation vapor pressure of condensate droplet, latent heat and coefficients were given on referring to Refs.(Sislian, 1975; Adam, 1996). Validation of condensation model using these equations and quantities was shown in Ref. (Matsuo, 2003).

At the inflow boundary upstream of the nozzle, all variables were fixed at the initial values and all variables are extrapolated at the outflow boundary downstream of nozzle. The non-slip wall condition was used on the solid surface. The Axisymmetric condition was used at the boundary of the nozzle center line. Iso-pressure and no heat transfer were constrained on the solid wall. Condensate mass fraction was set at $g = 0$ on the wall.

Computational conditions

Axisymmetric supersonic impinging jet flows driven by the sonic flow of a convergent nozzle (Addy, 1981) with a circular arc of R=12.7 mm are considered in the present computation, as sketched in Fig. 1. The nozzle exit diameter ϕD is 12.7 mm (characteristic length). The nozzle exit to impinging plate distance L is fixed at 31.75 mm (L/D=2.5). The number of grids is 70×60 (Δx_{min}=0.005D, Δy_{min}=0.0004D) in the nozzle region and 125 × 131 (Δx_{min}=0.0025D, Δy_{min}=0.0004D) in the jet plume and impingement region. Two nozzle pressure ratios, the ratio of the reservoir pressure p_0 (atmospheric pressure) to back pressure p_b ($=p_0/p_b$), 3.0 and 4.5 are used in the present calculation. Values of the initial degree of supersaturation, S_0 are 0 (dry air), 0.4 (moist air), 0.6 (moist air) and 0.8 (moist air). Total temperature T_0 and total pressure p_0 in the reservoir are 298.15 K and 101.3 kPa, respectively.

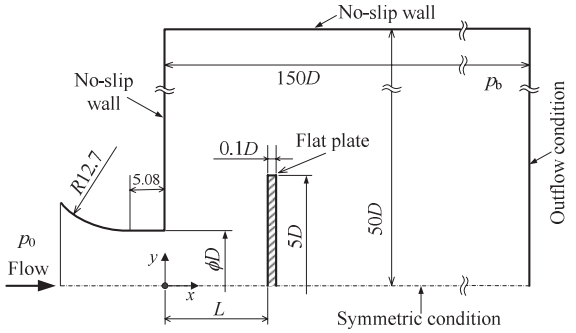

Figure 1: Computational domain and boundary conditions

EXPERIMENTAL APPARATUS AND METHOD

Experiments were conducted in order to verify the validity of the present computational work. A supersonic indraft wind tunnel where dry air at atmospheric pressure drawn into a vacuum tank, was used in the present experiment. Test section is a rectangular box which has a length of 553 mm, a width of 126 mm, and a height of 126 mm. A sonic nozzle (Addy, 1981) was set at the end of upper stream in the box. The reservoir pressure p_0 and back pressure p_b are

Table 1: Dominant frequency of the surface pressure oscillations (kHz)

	Nozzle to plate distance (L/D)		
	2.0	2.5	3.0
Computation	12.50	17.61	15.06
Experiment	11.61	17.37	14.67

the same as computational ones. Variations of surface pressure were measured using a pressure sensor installed at the center of the impinging plate. The flow field was investigated by a schlieren optical method.

RESULTS AND DISCUSSIONS

Comparison with experimental results

Dominant frequency of the surface pressure oscillations obtained from computations and experiments at the center (y/D=0) of impinging plate is shown in Table 1 for various nozzle-to-plate distance ratios (L/D). As seen from the table, the frequencies of the present computation are in good agreement with those of experiments.

Simulation of jet structure

Static pressure variations along the jet centerline are shown in Figs.2(a) and (b) during one period of flowfield oscillations for cases of p_0/p_b=3.0 and 4.5, respectively (S_0=0). From Fig. 2(a), it is found that the pressure distribution of the expansion region in the first cell from the nozzle exit, characterized by a monotonic decrease, does not vary with time. However, the pressure distribution over the compression region in the first cell and the region beyond are changes with time. In Fig.2(a), t=0.75T (T : periodic time of oscillation) refers to the instant when the pressure behind the first compression shock (near x/D=1.0) becomes the largest, and at the instant t=0.0T behind the first compression region, the pressure distribution becomes the smallest. This suggests that the shock cell structures change continuously during the cycle of oscillation. The nozzle pressure ratio, p_0/p_b, important operating parameter, affects the flow characteristics: the shock cell structure in an underexpanded jet is also varied with the nozzle pressure ratio. From Fig. 2(b), the length of the first shock cell increases with the increment of the nozzle pressure ratio and monotonic pressure distribution are shown in the first shock cell.

Figures 3(b) and (b) illustrate instantaneous flowfields (Mach number and pressure contours) corresponding to instant t=0.75T. In both cases, the jet has two cells and the plate shock is located behind the second expansion region. At the nozzle pressure ratio, p_0/p_b=4.5, a strong normal shock (Mach disk) develops in the first cell, as shown in Fig. 3(b). The flow downstream of the Mach disk becomes subsonic, and therefore, the strength of the plate shock behind the second expansion region becomes weaker. Figure 4 shows time histories of static pressure and distributions of power spectrum density at the center of the plate for p_0/p_b=3.0 and 4.5 (S_0=0). As is evident from Figs.4(b) and (d), peak values are observed in each cases. In addition, these figures indicate that the amplitude of pressure oscillations decreases with the nozzle pressure ratio from 3.0 to 4.5. This is in close agreement with the previous numerical observation of (Kim and Park, 2003).

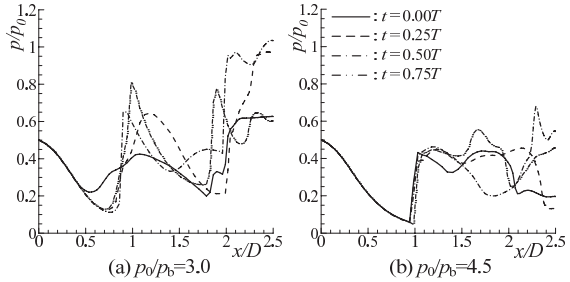

Figure 2: Variations of static pressure distribution along jet axis (S_0=0)

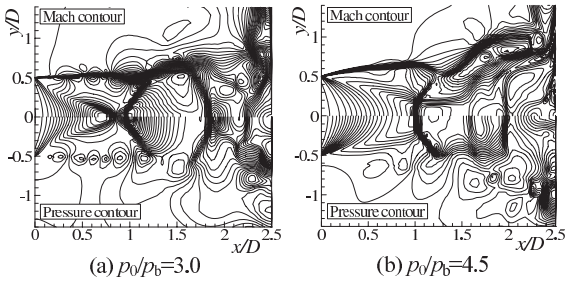

Figure 3: Instantaneous flowfields at instant t=0.75T(s) (S_0=0)

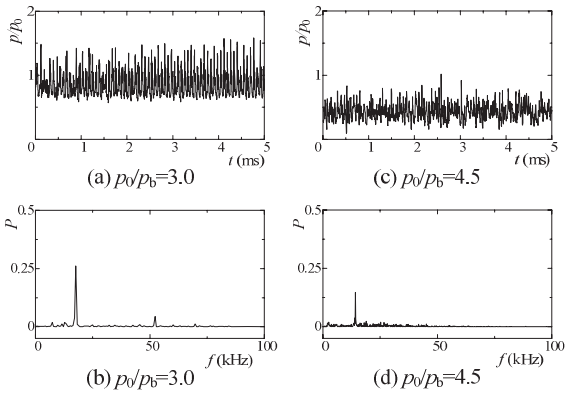

Figure 4: Time history of static pressure (a,c) and power spectrum density (b,d) (y/D=0, S_0=0)

Effect of non-equilibrium condensation

Figures 5, 6 and 7 show variations of distribution of static pressure p, condensate mass fraction g and nucleation rate I on the jet axis during one period of oscillation for p_0/p_b=3.0 (S_0=0.6), p_0/p_b=4.5 (S_0=0.4) and p_0/p_b=4.5 (S_0=0.8), respectively. As seen from Figs.5(a), 6(a) and 7(a), the amplitudes of static pressure during flowfield oscillation become smaller compared to that of without the non-equilibrium condensation (Figs. 2(a) and (b)). In addition, the amplitude of static pressure during flowfield oscillation become smaller with the increase in the initial degree of supersaturation (S_0), in Figs. 6(a) and 7(a). This implies, the increase in the initial degree of supersaturation results the higher amount of non-equilibrium condensation in the flowfield, and therefore, the pressure amplitude become lower.

From Figs.5(c), 6(c) and 7(c), the nucleation rate begins to increase from upstream of the nozzle exit and reaches the maximum at onset of condensation. Moreover, the condensate mass fraction begins to increase at the onset of con-

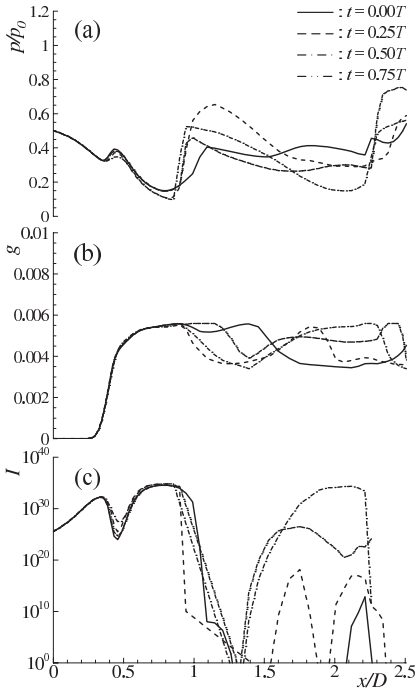

Figure 5: Variation of static pressure, condensate mass fraction and nucleation rate along jet axis (p_0/p_b=3.0, S_0=0.6)

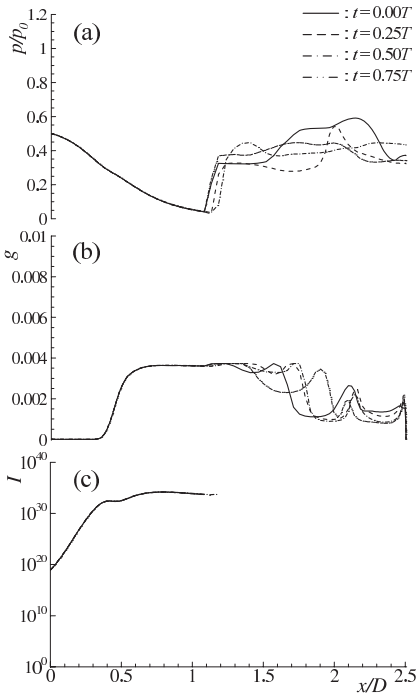

Figure 6: Variation of static pressure, condensate mass fraction and nucleation rate along jet axis (p_0/p_b=4.5, S_0=0.4)

densation as shown in Figs.5(b), 6(b)and 7(b). For all cases of S_0=0.4, 0.6 and 0.8 (p_0/p_b=3.0 and 4.5), the variation of static pressure, condensate mass fraction and nucleation rate are almost in same fashion. In both cases of p_0/p_b=3.0 and 4.5, the amplitude of static pressure during oscillation are reduced more with the increase in initial degree of supersaturation, S_0.

Instantaneous flowfields corresponding to instant t=0.25T, t=0.75T and t=0.50T, are shown in Figs.8, 9 and 10, respectively. In Fig. 8(a), p_0/p_b=3.0, S_0=0.6, the strength of the plate shock wave become weaker in comparison with the case of without non-equilibrium condensation. At the nozzle pressure ratio, p_0/p_b=4.5 and in all cases of S_0=0.4, 0.6 and 0.8, the plate shock behind the second expansion region disappears due to the effect of non-equilibrium condensation, in Figs. 9(a) and 10(a). From Figs. 8(b), 9(b) and 10(b), condensate nuclei begin to generate from the region upstream of the nozzle exit. The condensate mass fraction begins to increase rapidly in expansion fan and jet boundary.

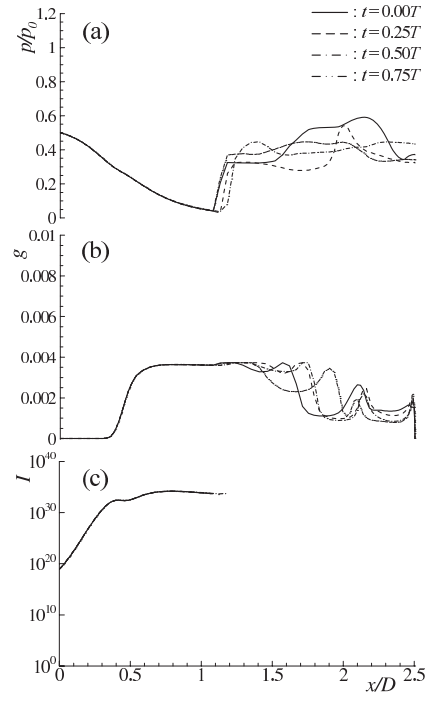

Figure 7: Variation of static pressure, condensate mass fraction and nucleation rate along jet axis (p_0/p_b=4.5, S_0=0.4)

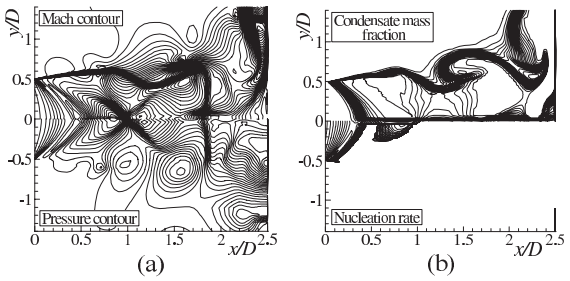

Figure 8: Instantaneous flowfields at instant t=0.25T(s) (p_0/p_b=3.0, S_0=0.6)

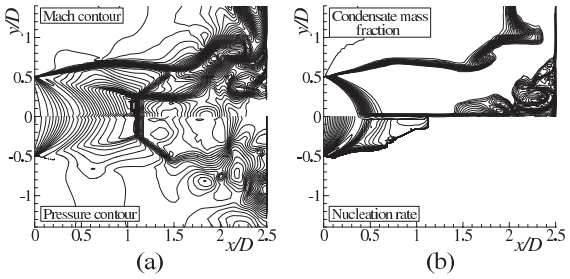

Figure 9: Instantaneous flowfields at instant t=0.75T(s) (p_0/p_b=4.5, S_0=0.4)

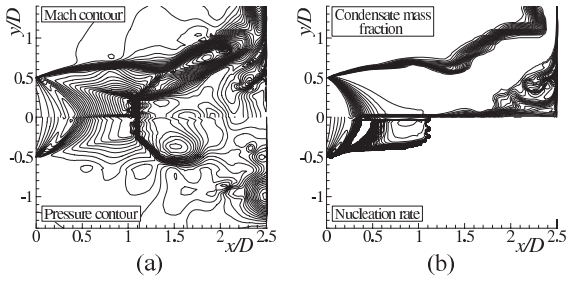

Figure 10: Instantaneous flowfields corresponds to instant t=0.50T(s) (p_0/p_b=4.5, S_0=0.4)

Figure 11 shows amplitudes of the surface pressure oscillation Δp and variations of the plate shock position Δx_s for both cases of p_0/p_b=3.0 and 4.5 (S_0=0.0, 0.4, 0.6 and 0.8). The amplitude of surface pressure denotes the difference between the maximum and the minimum pressure during one cycle of flowfield oscillation at the center (y/D=0) of impinging plate. The plate shock position x_s is measured from the impinging plate to the plate shock. When a supersonic jet impinges perpendicularly on a flat plat, a strong normal shock (plate shock) appears over the plate. In the oscillatory case, the plate shock moves to and fro along the jet axis like a plane shock oscillation. The frequencies of the plate shock oscillations are identical with those of the surface pressure oscillations. Furthermore, as seen from Fig.3(a) and (b), the flow field between an oscillatory plate shock wave and the vertical plate has very complicated structure. The interaction between a jet boundary with high vorticity fluid and an oblique shock wave seems to have strong effects on the flow field. From this figure, in both cases of p_0/p_b=3.0 and 4.5, increment of initial degree of supersaturation S_0 results to the reduction of the amplitude of surface pressure oscillations due to the occurrence of non-equilibrium condensation of the moist air. In addition, the occurrence of non-equilibrium condensation reduces the excursion region, means the to and fro motion, of the plate shock. At nozzle pressure ratio p_0/p_b=4.5, in moist air flow the zero values of x_s indicate the disappearance of the plate shock wave.

Jet entrainment velocities in the near aerodynamic field are the key measure of lift loss, in STOVL aircraft while in hover mode. The entrainment of the ambient fluid by the primary lifting jet(s) induces low pressures on the lower surface of the airframe, which in the present configuration is represented by a circular plate at nozzle exit. Additional entrainment by the radial wall jet also formed because of the impingement of the jet can further reduce the surface pressures on the lift plate. It is expected that the entrainment due to the wall jet will become more significant when the impinging plane is in close proximity to the nozzle exit and the ambient region from which the fluid is entrained becomes increasingly confined. As a result of the low surface pressures, a force in a direction opposite to the jet thrust is created, leading to a lift loss. Typical instantaneous velocity variations at a radial location of 1.5D are shown in Fig.12. Included in this figure is the data for dry and moist air jet impingement at nozzle pressure ratio, p_0/p_b of 3.0 and 4.5, respectively. The magnitude of the near-field instantaneous entrainment velocity, q ($q = \sqrt{(u^2 + v^2)}$) for dry air jet impingement is higher compared with the moist air jet impingement, as indicated by the peaks in the velocity plot. Such large velocities in the near aerodynamic field, in case of dry air, correspond to the presence of large vortical structures. Other hand, in case of moist air jet impingement, the occurrence of non-equilibrium condensation reduces the magnitude of entrainment which corresponds to the reduction of turbulent fluctuations in the jet shear layer region.

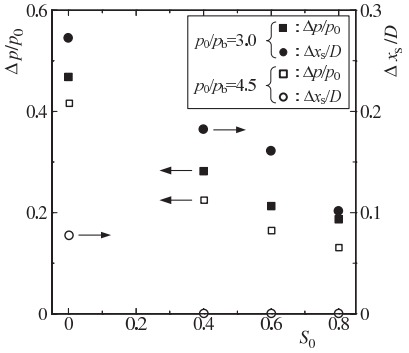

Figure 11: The amplitudes of the surface pressure and the plate shock oscillations

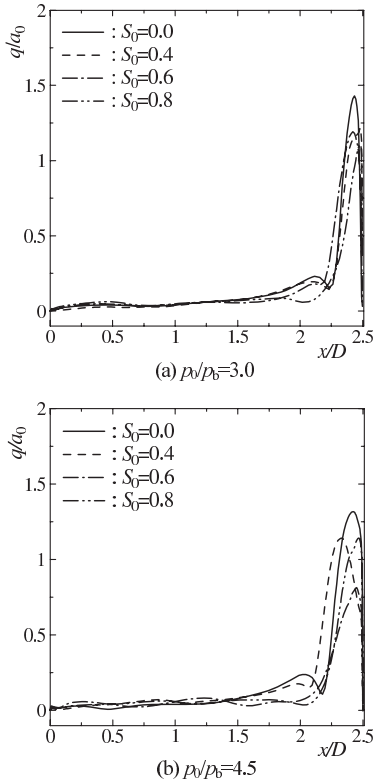

Figure 12: Instantaneous entrainment velocity at a radial location of y/D=1.5. (a) p_0/p_b=3.0; (b) p_0/p_b=4.5

Figures 13 and 14 show time histories of static pressure and distributions of power spectrum density at the center (y/D=0) of impinging plate for the cases of p_0/p_b=3.0 and 4.5, respectively (S_0=0.4, 0.6 and 0.8). For both cases of p_0/p_b=3.0 and 4.5, amplitudes of static pressure for S_0=0.4, 0.6 and 0.8 (Figs.13(a,c,e) and 7(a,c,e)) become small compared with those of S_0=0 (Fig.4(a,c))and peaks of the power spectrum density are reduced in case with non-equilibrium condensation (in Figs.13(b,d,f) and 14(b,d,f)). Furthermore, in both cases (p_0/p_b=3.0 and 4.5), the amplitude of static pressure and peaks of the power spectrum density are reduced with the increase of the initial degree of supersaturation, S_0. This means that energy of turbulent fluctuations is reduced due to relaxation processes of evaporation and con-

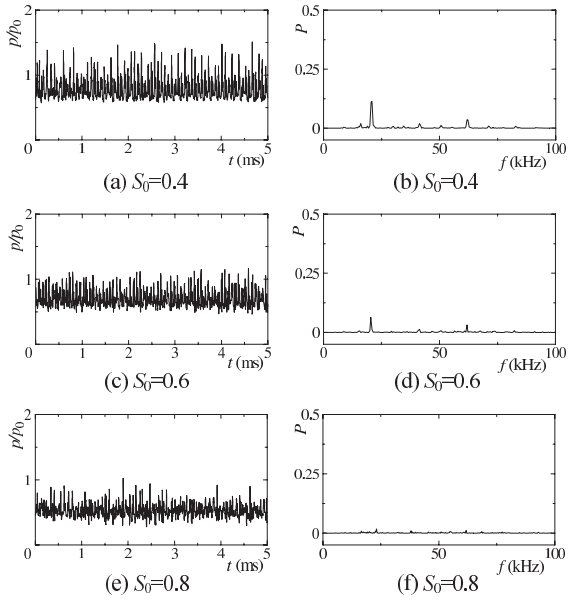

Figure 13: Time history of static pressure (a,c,e) and power spectrum density (b,d,f)(p_0/p_b=3.0, y/D=0)

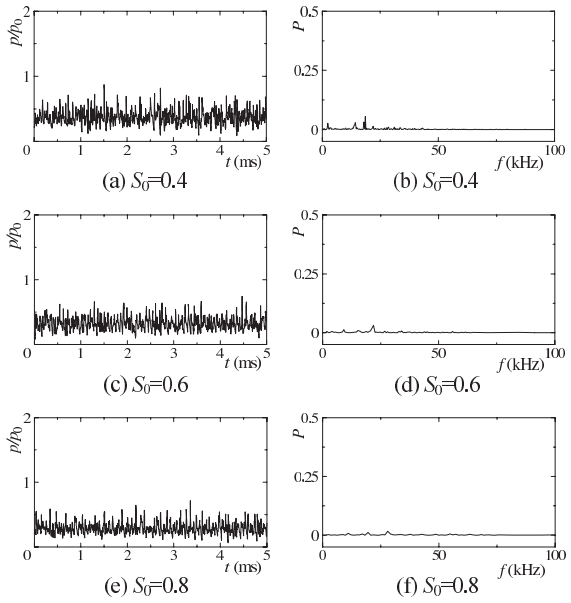

Figure 14: Time history of static pressure (a,c,e) and power spectrum density (b,d,f)(p_0/p_b=4.5, y/D=0)

densation of vapor molecules on small droplet surface (Hiller et al., 1971). Therefore, this shows that the occurrence of non-equilibrium condensation enable one to reduce the noise level of supersonic impinging jets.

CONCLUSIONS

In the present study, the axisymmetric unsteady Navier-Stokes equations system with coupled droplet growth equation was used to investigate the oscillatory features of surface pressure and the structural change of the supersonic under-expanded moist air jet impinging on a flat plate by varying the nozzle pressure ratio. Furthermore, the numerical results were compared with experimental results. The results obtained are summarized as follows: in the case with non-equilibrium condensation, the amplitude of pressure oscillation become small compared with those of dry air, and peaks of the power spectrum density are reduced in case with non-equilibrium condensation. The occurrence of non-equilibrium condensation reduces the magnitude of entrainment velocity which corresponds to the reduction of lift loss.

REFERENCES

Petrie, A.M., 1980, "An experimental investigation of jet screech by air jet impingement on solid boundaries", *Applied Scientific Research*, Vol.36, pp.93-108.

Lamont, P.J., Hunt, B.L., 1980, "The impingement of underexpanded, Axisymmetric jets on perpendicular and inclined flat plates", *Journal of Fluid Mechanics*, Vol.100, part 3, pp. 471-511.

Kim, S.I., Park, S.O., 2005, "Oscillatory behavior of supersonic impinging jet flows", *Shock Waves*, Vol.14, part 4, pp.259272.

Krothapalli, A., 1985, "Discrete tones generated by an impinging underexpanded rectangular jet", *AIAA Journal*, Vol.23, pp.1910-1915.

Powell, A., 1988, "The sound-producing oscillations of round underexpanded jets impinging on normal plates", *J. Acoust. Soc. Am.*, Vol.83, pp.515-533.

Tam, C.K.W., Ahuja, K.K., 1990, "Theoretical model of discrete tone generation by impinging jets", *J. Fluid Mechanics*, Vol.214, pp.67-87.

Wegener, P. P., Mack, L. M., 1958, "Condensation in supersonic hypersonic wind tunnels", *Adv. In Appl. Mech.*, 5, Academic Press.

Matsuo, K., Kawagoe, S., Sonoda, K., Sakao, K., 1985, "Studies of Condensation Shock Waves (part 1, Mechanism of their Formation)", *Bulletin of JSME*, Vol.28, pp.2577-2582.

Sislian, J. P., 1975, "Condensation of Water Vapor with or without a Carrier Gas in a Shock Tube", *UTIAS Report*, No. 201.

Goldberg, U. C., 1994, "Toward a Pointwise Turbulence Model for Wall-Bounded and Free Shear Flows", *ASME Journal of Fluids Engineering*, Vol.116, pp.72-76.

Goldberg, U. C., 1996, "Exploring a Three-Equation $R-k-e$ Turbulence Model", *ASME Journal of Fluids Engineering*, Vol.118, pp.795-799.

Heiler, M., 1999, Instationre Phnomene in Homogen/Heterogen Kondensierenden Dsen- und Turbinenstrmungen, Dissertation, Fakultt fr Maschinenbau, Universitt Karlsruhe (TH), Germany.

Adam, S., 1996, Numerische und Experimentelle untersuchung Instationrer Dsenstrmungen mit Energiezufuhr durch Homogene Kondensation, Dissetation, Fakultt fr Maschinenbau, Universitt Karlsruhe (TH), Germany.

Matsuo, S., Tanaka, M., Setoguchi, T., Kaneko, K., 2003, "Effect of Non-Equilibrium Condensation of Moist Air on Flow Fields in Ludwieg Tube (Case without Condensation Upstream of Nozzle)", *Trans. Jpn. Soc. Mech. Eng.*, (in Japanese), Vol.69, No.681, pp.1163-1170.

Yee, H. C., 1989, "A class of high-resolution explicit and implicit shock capturing methods", *NASA TM-89464*.

Addy, A.L., 1981, "Effects of Axisymmetric Sonic Nozzle Geometry on Mach Disk Characteristics", *AIAA Journal*, Vol.19, No.1, pp.121-122.

Hiller, W.J., Jaeschke, M., Meier, G.E.A., 1971, "The influence of Air Humidity on Pressure and Density Fluctuations in Transonic Jets", *J. Sound Vib.*, Vol.17, No.3, pp.423-428.